Current Measurement of Three-Core Cables via Magnetic Sensors

Jingang Su [1,*], Peng Zhang [1], Xingwang Huang [1], Xianhai Pang [1], Xun Diao [2] and Yan Li [2]

1   Electric Power Research Institute, State Grid Hebei Electric Power Supply Co., Ltd., Shijiazhuang 050021, China; hbdyyzp@163.com (P.Z.); huangxingwang1997@163.com (X.H.); dyy_pangxh@126.com (X.P.)
2   Department of Electrical Engineering, North China Electric Power University (Baoding), Baoding 071003, China; diaoxun2001@163.com (X.D.); yan.li@ncepu.edu.cn (Y.L.)
*   Correspondence: sujingang@tju.edu.cn

Abstract: Due to their compact structure and low laying cost, three-core power cables are widely used for power distribution networks. The three-phases of such cables are distributed symmetrically with a 120° shift to each other. Phase current is an important parameter to reflect the operation state of the power system and three-core cable. Three-core symmetrical power cables use a common shield, leading to magnetic field cancelation outside the cable during steady operation. Thus, traditional magnetic-based current transformers cannot measure the phase current on three-core cable non-invasively. In order to measure the phase current more conveniently, a phase current measurement method for three-core cables based on a magnetic sensor is proposed in this paper. Nonlinear equations of a phase current and the magnetic field of a measuring point are constructed. The calculated magnetic field distribution of the three-core cable is verified using a finite element simulation. The effectiveness of the measurement method is further validated through experiments. This proposed method is able to conveniently detect the phase current of three-core power cables, which can help cable maintenance.

Keywords: three-core cable; current measurement; magnetic sensor; phase current

1. Introduction

With the development of urbanization, transmission and distribution corridors become increasingly tense. Therefore, the construction of urban transmission lines is of great significance to meet the needs of urban economic development [1]. In the construction of urban transmission lines, due to the scarcity of urban land resources, the transmission corridors of overhead lines are often tense, and the construction of overhead lines affects the urban landscape. In the construction of urban transmission lines, transmission cables with a high utilization rate of transmission corridors and high environmental friendliness are often used. In this case, the safe operation of power cables becomes critical. In terms of distribution cables, compared with single-core cables, three-core symmetrical power cables are favored in medium-low voltage (below 35 kV) distribution projects due to their lower cost [2]. The current is one of the most important electrical state quantities, and the current can reflect the running state of the three-core cable, so the phase current measurement of cables is of great significance [3].

Current monitoring has been investigated by different researchers. With the development of magnetic measurement technology, the use of magnetic sensors to measure current has become a method recognized by the power industry. Reference [4] designed a circular magnetic field sensor array with a 45° difference for the arc current of a single-core cable. In reference [5], a current sensor composed of three Hall sensors with a difference of 120° is constructed, and a method of single-conductor current measurement is proposed. Reference [6] designed a Hall sensor with a phase difference of 90° to measure the current

of a single conductor. Reference [7] proposed a method to measure the magnetic field of an 11 kV single-core cable with a linear giant reluctance array. Compared with the ferromagnetic current transformer, this method improved the accuracy. However, the measurement object of the above literature is the current of single conductor, and it is not suitable for multi-conductor systems such as three-core cables.

In general, phase A, phase B, and phase C are distributed symmetrically with a 120° difference in the three-core power cable [8]. Due to such geometry, traditional current measurement methods based on an electromagnetic induction principle are not suitable, since the magnetic field cancels out around the surface of the cable.

For the three-core cable, reference [9] designed a giant magnetoresistance sensor to monitor the charging status, but the method of current measurement is not given in the paper. Reference [10] proposed an analytical calculation method for the surface magnetic field of three-core cables. However, this method requires three magnetic sensors to be installed at specific positions, which limits its application.

In this paper, the mathematical model of the phase current and magnetic field around three-core cables is established based on the Ampere theorem. By arranging multiple sensors around the cable to measure the magnetic field, the phase current in the three-core cable can be effectively measured via an inversion model. The proposed methodology is validated through a test.

2. Materials and Methods

The structure of the general three-core cable is shown in Figure 1, and the parameters are shown in Table 1.
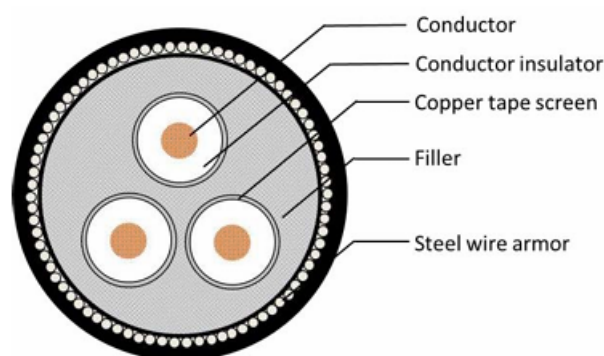

Figure 1. Three-core cable structure.

Table 1. Three-core cable structure parameters.

Structure	Radius/mm	Materials
Conductor	8.32	Copper
Conductor insulator	12.84	XLPE
Copper tape screen	15.99	Copper
Filler	26.2	Polythene
Steel wire armor	2.56	Steel

The surface magnetic flux density of the three-core cable rotates with the phase current. And the surface magnetic field is the vector superposition of the three-phase current magnetic field. Since the distance from a particular point on the surface of the cable to the three cores is different, the superimposed magnetic field is not perfectly zero [11].

In this paper, four magnetic sensors are used for phase current measurement. The sensors are numbers S_1–S_4 and placed on the surface of the three-core cable. As shown in Figure 2, point O is the center of the three-core cable while points A, B, and C are the centers of phase A, B, and C cores, respectively. The distance between point O and the center of each core is r_A, r_B, and r_C. The radius of the cable is R. The angle between OA, OB,

OC, and the *x* axis forward is α, β, γ, respectively, with 120° difference. The coordinates of points A, B, and C can be obtained as $(r_A \cos\alpha, r_A \sin\alpha)$, $(r_B \cos\beta, r_B \sin\beta)$, and $(r_C \cos\gamma, r_C \sin\gamma)$, respectively.
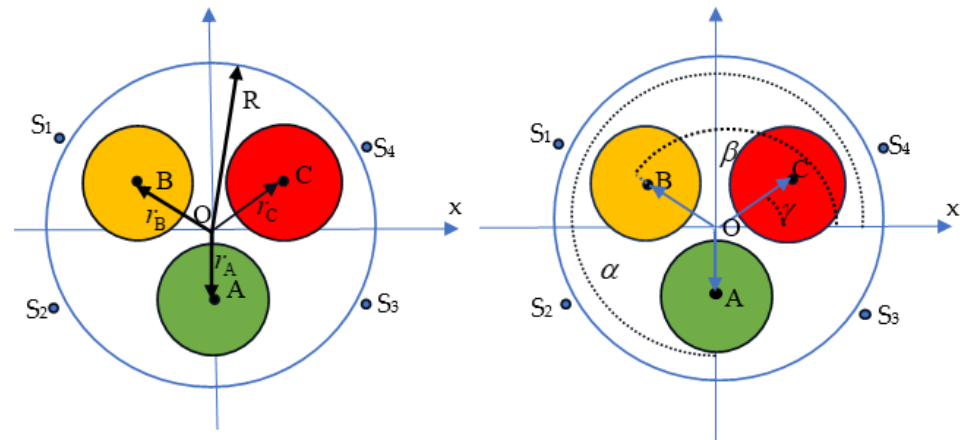

Figure 2. Schematic of surface magnetic field-sensing model for three-core cable.

The magnetic flux density B_1–B_4 along the tangential direction generated at S_1–S_4 can be obtained, as shown in Equations (1)–(4) [12]. In the equations, μ represents the permeability of the vacuum. The three-phase current I_A, I_B, I_C, and rotation angle α are unknown. The cable radius R, the distance between the cable center and the three-phase core center r_A, r_B, r_C, and the magnetic flux density measured using the magnetic sensor are known. The number of unknowns in the equations is smaller than the number of equations, which makes the equations overdetermined. And the phase current of the cable can be obtained by solving the equations. The surface magnetic field of a three-core cable is a vector superposition of each current magnetic field. The equations of tangential magnetic flux density can be derived from the Ampere-loop theorem [12]. Taking Equation (1) as an example, the three parts in Equation (1) are the magnetic flux density of each current at S_1, and the total magnetic flux density can be obtained by superimposing them.

$$B_1 = \frac{\mu}{2\pi} \left[\frac{R - r_A \sin(\alpha - 60°)}{R^2 + r_A^2 - 2Rr_A \sin(\alpha - 60°)} I_A + \frac{R - r_B \sin(\alpha - 180°)}{R^2 + r_B^2 - 2Rr_B \sin(\alpha - 180°)} I_B + \frac{R - r_C \sin(\alpha + 60°)}{R^2 + r_C^2 - 2Rr_C \sin(\alpha + 60°)} I_C \right] \quad (1)$$

$$B_2 = \frac{\mu}{2\pi} \left[\frac{R - r_A \sin(\alpha - 120°)}{R^2 + r_A^2 - 2Rr_A \sin(\alpha - 120°)} I_A + \frac{R - r_B \sin(\alpha + 120°)}{R^2 + r_B^2 - 2Rr_B \sin(\alpha + 120°)} I_B + \frac{R - r_C \sin\alpha}{R^2 + r_C^2 - 2Rr_C \sin\alpha} I_C \right] \quad (2)$$

$$B_3 = \frac{\mu}{2\pi} \left[\frac{R - r_A \sin(\alpha + 120°)}{R^2 + r_A^2 - 2Rr_A \sin(\alpha + 120°)} I_A + \frac{R - r_B \sin\alpha}{R^2 + r_B^2 - 2Rr_B \sin\alpha} I_B + \frac{R - r_C \sin(\alpha - 120°)}{R^2 + r_C^2 - 2Rr_C \sin(\alpha - 120°)} I_C \right] \quad (3)$$

$$B_4 = \frac{\mu}{2\pi} \left[\frac{R - r_A \sin(\alpha + 60°)}{R^2 + r_A^2 - 2Rr_A \sin(\alpha + 60°)} I_A + \frac{R - r_B \sin(\alpha - 60°)}{R^2 + r_B^2 - 2Rr_B \sin(\alpha - 60°)} I_B + \frac{R - r_C \sin(\alpha + 180°)}{R^2 + r_C^2 - 2Rr_C \sin(\alpha + 180°)} I_C \right] \quad (4)$$

Because of the sinusoidal term of rotation angle α, the equations are nonlinear. It is impossible to obtain a specific expression for the phase current based on magnetic flux density. The problem can be solved numerically to obtain the current. The nonlinear least square method is used to approximate the optimal solution. The phase currents for the three-core cable can be obtained using this method.

In this paper, Newton–Raphson algorithm is used for the nonlinear least square method. The algorithm is the result of Taylor expansion and the approximation of nonlinear equations. For a given function $f(x)$ (least square between actual magnetic flux density and estimated magnetic flux density), x_0 is the approximate root of the function and $f'(x)$ is the first derivative of the function. The function is considered to be locally linearized near

x_0. The specific equation is shown below. The final result is obtained through continuous iteration, where n is the iteration number.

$$f(x) \approx 0 \approx f(x_0) + f'(x_0)(x_1 - x_0) \tag{5}$$

$$x_1 = x_0 - \frac{f(x_0)}{f'(x_0)} \dots\dots \tag{6}$$

$$x_{n+1} = x_n - \frac{f(x_n)}{f'(x_n)} \tag{7}$$

In order to show the magnetic field distribution, the finite element method is used for the magnetic field analysis. The parameters in Table 1 are used for the simulation. Furthermore, the frequency in the simulation is 50 Hz. The current amplitude is 707.1 A. The three–phase currents differ by 120° in the phase. The mesh diagram with triangles is shown in Figure 3. The governing equations to analyze the magnetic field are shown in Equations (8)–(11). The result is shown in Figure 4. Along the surface red route indicated in Figure 4, the magnetic flux density around the cable is extracted and shown in Figure 5.

$$\nabla \times H = J \tag{8}$$

$$B = \nabla \times A \tag{9}$$

$$J = \sigma E + j\omega D \tag{10}$$

$$E = -j\omega A \tag{11}$$

where H represents the magnetic intensity, J represents the conducted current density, D represents the electric displacement, E represents the electric field intensity, A represents the magnetic potential, and σ represents the conductivity.
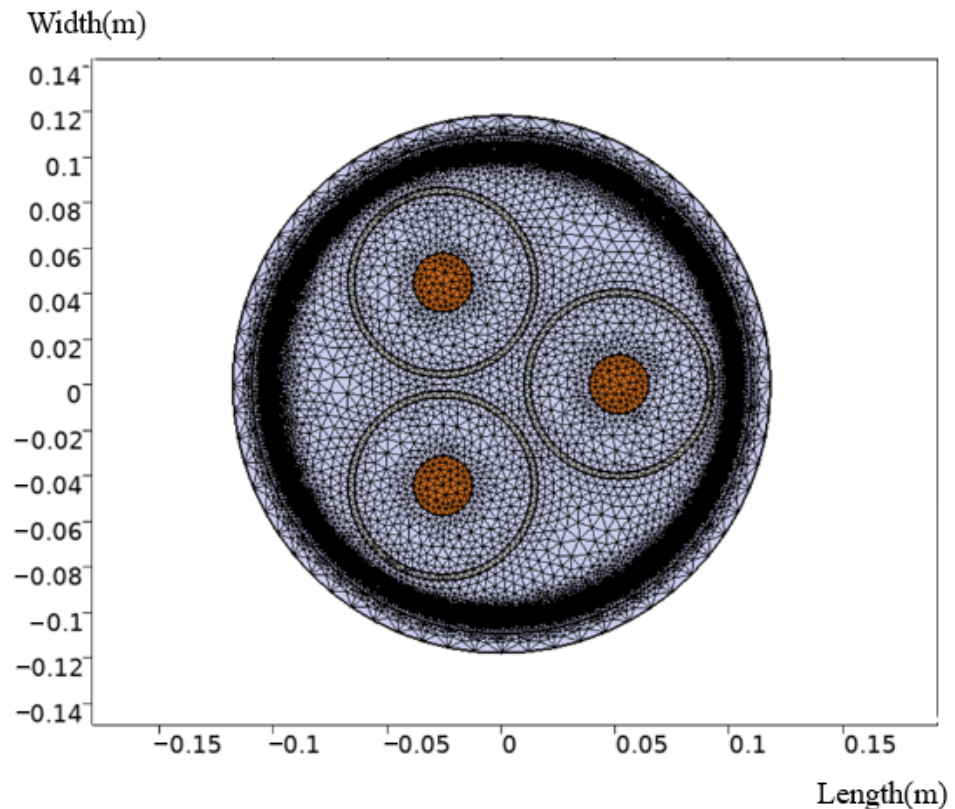

Figure 3. Mesh diagram of finite element simulation for cable magnetic field.

Figure 4. Finite element simulation result of magnetic field profile.
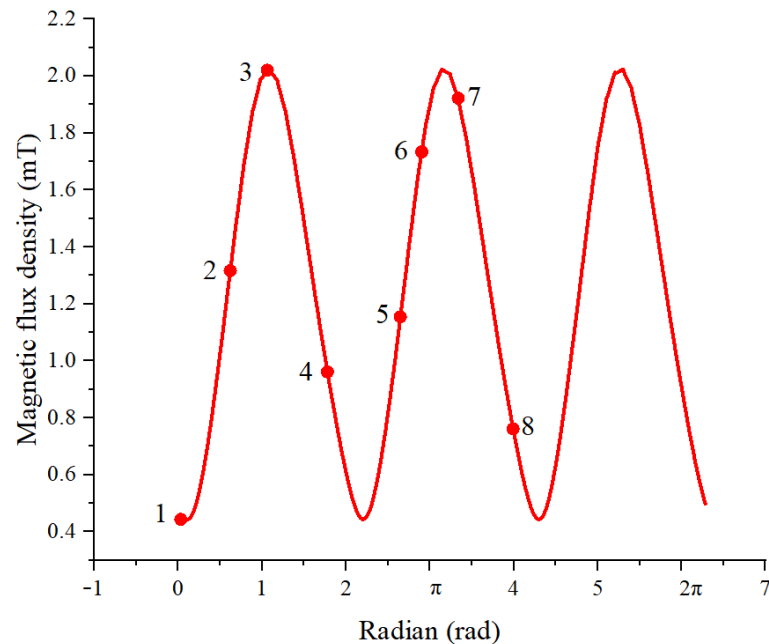
Figure 5. Simulation result of magnetic flux density along radian.

As can be seen from Figure 4, the magnetic field can be observed outside the cable, since the distances from the cable outer surface to three cores are different. The magnetic flux density is not evenly distributed at the measuring positions of the magnetic sensors. It can be seen from Figure 5 that the magnetic flux density of the surface rotates as the location changes, with a maximum value occurring every 120°. Eight different points are selected in Figure 5. The magnetic flux density results derived using Equations (1)–(4)

and the finite element method are shown in Table 2. The comparison shows that the error is about 2%, which confirms the accuracy of Equations (1)–(4). The main reason for the error is that there is a skin effect and a proximity effect, which makes the cable current distribution uneven.

Table 2. Comparison of simulation results and calculation results of magnetic flux density.

Serial Number	Simulation Result/mT	Calculation Result/mT	Error/%
1	0.44	0.45	2.4
2	1.28	1.29	1.3
3	2.02	2.05	1.4
4	0.98	0.96	2.4
5	1.16	1.18	1.4
6	1.72	1.76	2.2
7	1.92	1.96	2.1
8	0.76	0.74	2.6

As for the influence of steel wire armor on magnetic field distribution, the magnetic field simulation after removing the steel wire armor is performed in this paper, as shown in Figure 6.
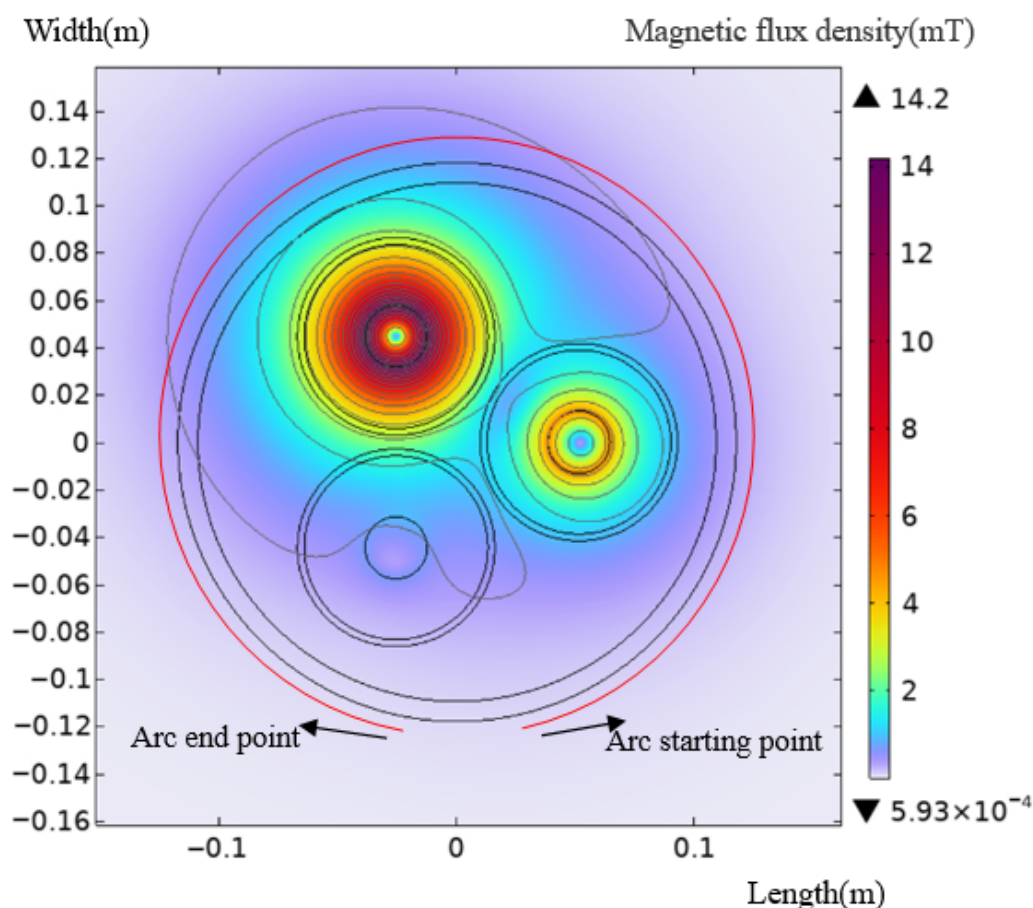

Figure 6. Finite element simulation of magnetic field without steel wire armor.

The magnetic flux density of the three-core cable without steel wire armor is shown in Figure 6. Since the three-core cable has a balanced current, the steel wire armor has little influence on the magnetic field distribution of the three-core cable, and it has little influence on the measurement results of the magnetic sensor. So, the magnetic field distribution in Figure 6 is almost identical to Figure 4.

3. Validation of Sensor's Performance via Single-Core Cable

In the follow-up experiment, the magnetic sensors will be used for the current measurement of the single-core cable. This aim of this section is to test the performance of the magnetic sensor and then verify whether the related experiments of the three-phase cables can be carried out. In the experiment, the cable is long enough to be considered as an infinite straight wire. The magnetic sensor used is the commercial TMR2905 model [13]. It is produced by MultiDimension Technology Co., Ltd., which located in Jiangsu, China.

For a single-phase wire, the relationship between its magnetic flux density and current is shown in Equation (12) [14].

$$B = \frac{\mu I}{2\pi x} \tag{12}$$

where μ represents the vacuum permeability, I represents the current energized in the wire, and x represents the distance between the measuring point and the wire. The sensitivity of the magnetic sensor used is 2 V/mT, and the corresponding magnetic field strength can be calculated by the voltage measured from the magnetic sensor. The magnetic flux density can then be used to derive the current based on Equation (12). The deduced current is compared with the actual current and the relative error can be calculated. Based on these results, Figure 7 is plotted for better visualization.
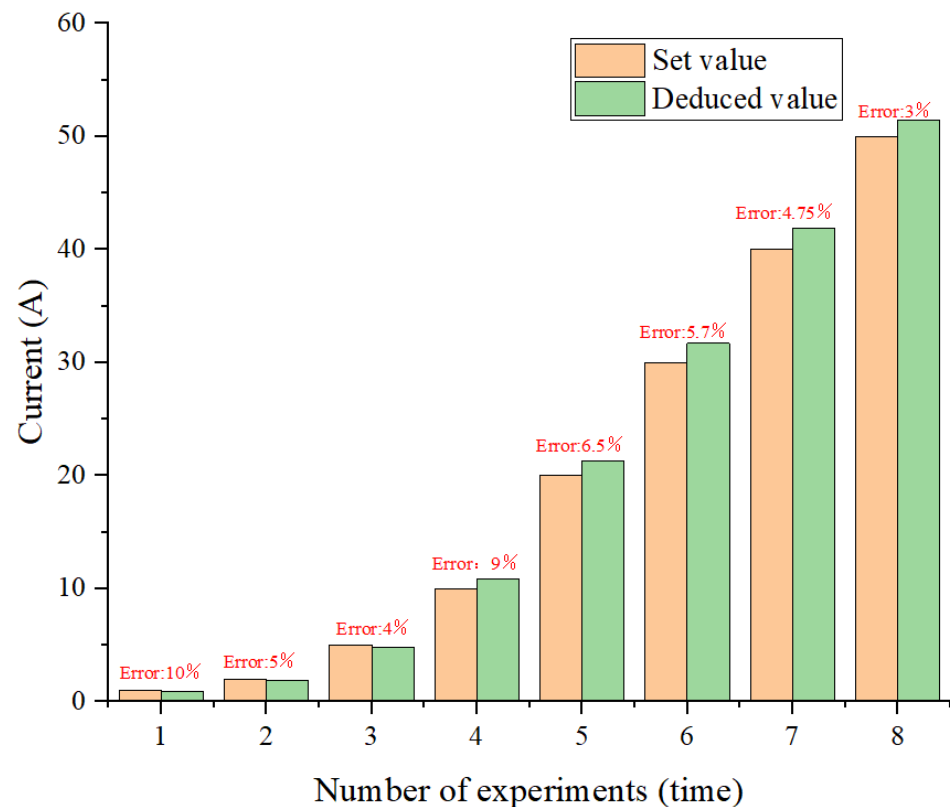

Figure 7. Set values and deduced values and errors of current.

It can be seen from Figure 7 that the error between the actual current results and the calculated results is less than 10%, indicating that this method is effective for the measurement of cable current, and when the current is greater than or less than 10 A, the larger the current, the smaller the experimental error. The errors are mainly instrumental errors and environmental errors. There are errors in the calibration and sensitivity of the instrument. In addition, the ambient temperature and air pressure will also affect the experimental results. This experiment lays a foundation for the phase current measurement of the following three-phase cable.

4. Three-Phase Cable Measurement

4.1. Test Setup

To obtain the phase current of the three-core cable, the measurement requires at least four sensors, as in Figure 2. The size data of the cables used are shown in Table 1. The experiment setup of the experiment is shown in Figure 8, while the schematic diagram is shown in Figure 9. One of the magnetic sensor results collected during the experiment is shown in Figure 10. Because the measurement results are a superposition of three currents, the data in Figure 10 are not a standard sinusoidal waveform. From these data, the magnetic flux density can be calculated from the sensor sensitivity (2 V/mT). And then the current magnitude can be calculated using Equations (1)–(4), as in Section 2.

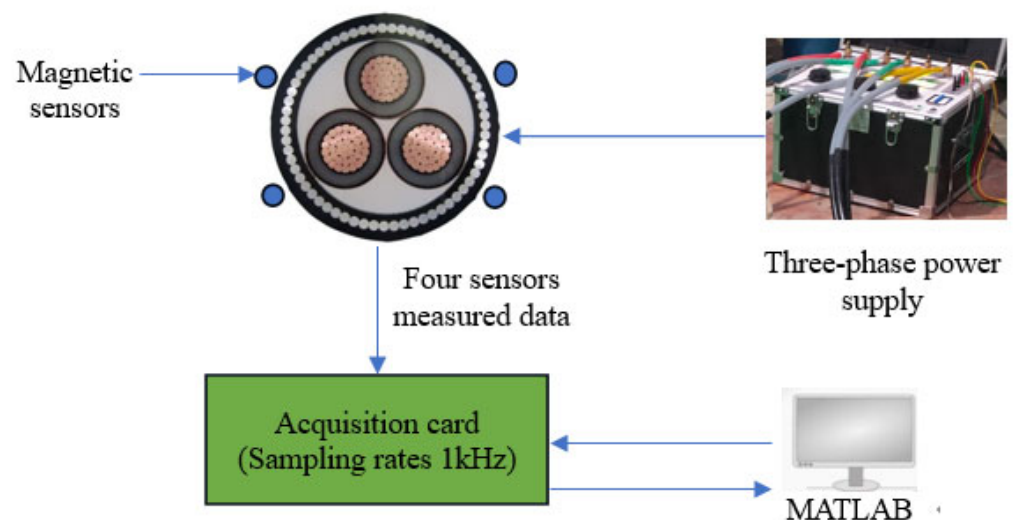**Figure 8.** Laboratory test picture for three-core cable current measurement with magnetic sensors.

Figure 9. Schematic drawing of the laboratory test.
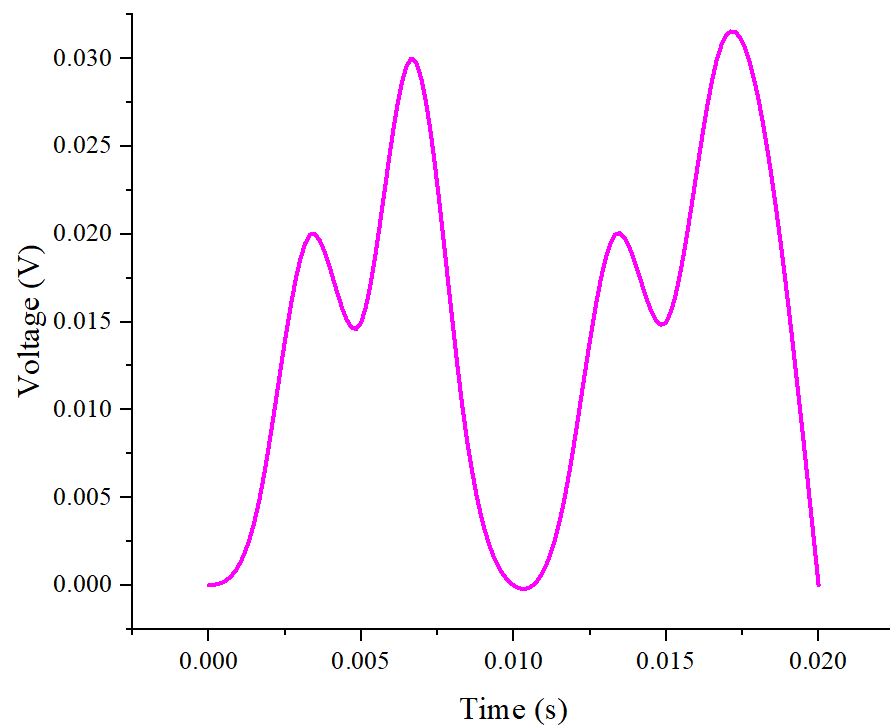
Figure 10. Part of the data collected by the experiment.

4.2. Test Result

This experiment loaded the three-core cable with phase current of 20 A, 30 A, and 60 A. By solving Equations (1)–(4) with the measured magnetic flux density, the deduced current can be obtained as shown in Figure 11. The working voltage of the magnetic sensor used is 3 V and the sensitivity is 2 V/mT. The working voltage of the information acquisition system is 4.5 V and the sampling rate is 1 kHz.
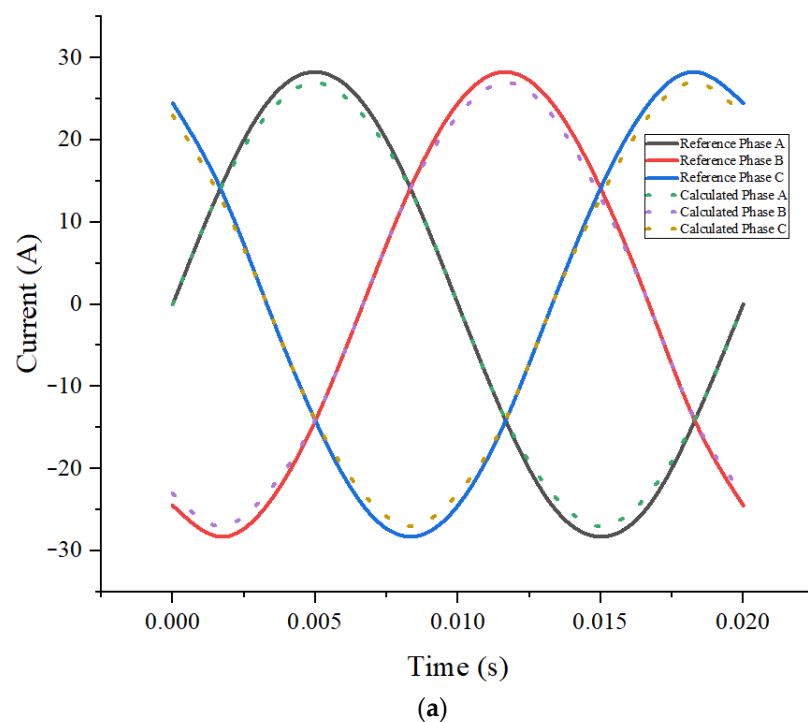

(a)

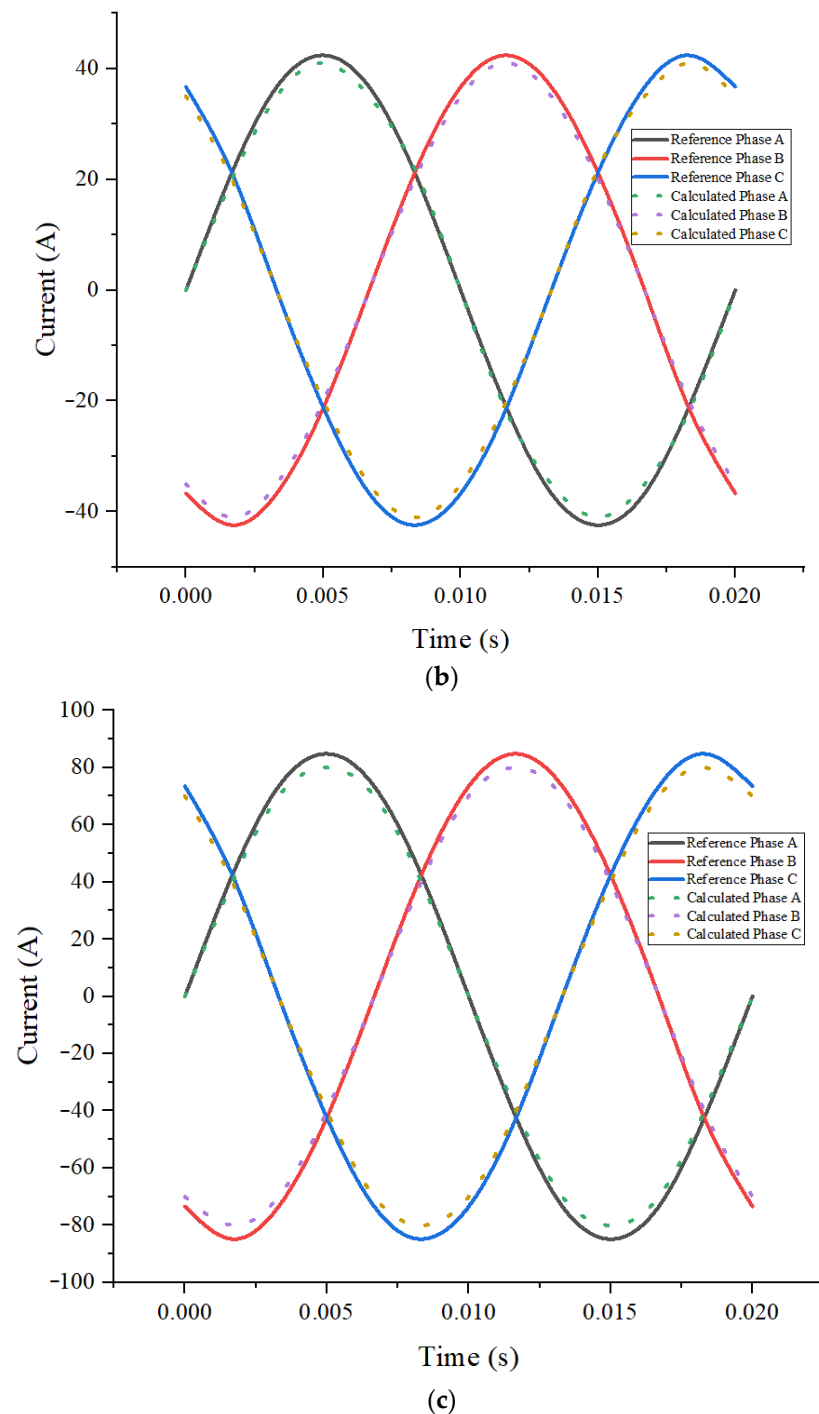**Figure 11.** *Cont.*

(b)

(c)

Figure 11. Experiment to derive the three-phase cable current. (**a**) Comparison between the calculated value and the reference value when the current is 20 A. (**b**) Comparison between the calculated value and the reference value when the current is 30 A. (**c**) Comparison between the calculated value and the reference value when the current is 60 A.

It can be seen that the derived current from the magnetic sensor (dashed line in Figure 11) is basically sinusoidally distributed, and the three-phase current difference is 120°. Compared with the real loaded reference current (solid line in Figure 11), the error between the two is about 6%, indicating that the current measurement method is effective.

The above method analyzes the three-phase current amplitude with the same value. In actual operation, the three-phase current will often appear as an imbalanced situation. Under this condition, the three-phase current should be regarded as the three unknowns.

Together with the angle α, a total of four unknowns need to be solved. In this case, a similar procedure can be performed with four magnetic sensors to derive the current values. For the case of simplicity, it is not shown in this paper.

5. Conclusions

Since the traditional magnetic field-based current measurement method cannot be used for the phase current of the three-core power cables, this paper introduces a three-core cable toroidal-surface magnetic field-sensing model. Based on such a model, the relationship between the cable surface magnetic field and the phase current is established. A phase current measurement method for three-core power cables based on magnetic sensors is proposed. At the same time, the imbalance of the three-phase current is analyzed and the solution is proposed. The validity of the model and the method is verified using simulation and experiment. The experimental error of this method is less than 6%, which verifies that the proposed method can be used for the phase-current sensing of three-core power cables.

References

1. Quiroga, O.A.; Melendez, J.; Herraiz, S. Fault causes analysis in feeders of power distribution networks. In Proceedings of the International Conference in Renewables Energies and Quality Power, Las Palmas de Gran Canaria, Spain, 13–15 April 2011; Volume 11.
2. Zhu, K.; Pong, P.W.T. Fault Classification of Power Distribution Cables by Detecting Decaying DC Components with Magnetic Sensing. *IEEE Trans. Instrum. Meas.* **2019**, *69*, 2016–2027. [CrossRef]
3. Bahador, N.; Namdari, F.; Matinfar, H.R. Tree-related high impedance fault location using phase shift measurement of the high-frequency magnetic field. *Int. J. Electr. Power Energy Syst.* **2018**, *100*, 531–539. [CrossRef]
4. Ametani, A. A general formulation of impedance and admittance of cables. *IEEE Trans. Power Appar. Syst.* **1980**, *3*, 902–910. [CrossRef]
5. Ukil, A.; Braendle, H.; Krippner, P. Distributed temperature sensing: Review of technology and applications. *IEEE Sens. J.* **2012**, *12*, 885–892. [CrossRef]
6. Marti, L. Simulation of transients in underground cables with frequency-dependent modal transformation matrices. *IEEE Trans. Power Deliv.* **1988**, *3*, 1099–1110. [CrossRef]
7. Lee, B. Review of the present status of optical fiber sensors. *Opt. Fiber Technol.* **2003**, *9*, 57–79. [CrossRef]
8. Liu, Z. Hall Drift Current Characteristics in the Experimental Study Hall Thruster. Master's Thesis, Harbin Industrial University, Harbin, China, 2022.
9. Sun, X.; Jiang, L.; Pong, P.W.T. Magnetic flux concentration at micrometer scale. *Microelectron. Eng.* **2013**, *111*, 77–81. [CrossRef]
10. Zhu, K.; Pong, P.W.T. Curved trapezoidal magnetic flux concentrator design for improving sensitivity of magnetic sensor in multiconductor current measurement. In Proceedings of the 2016 5th International Symposium on Next-Generation Electronics, Taiwan, China, 4–6 May 2016; pp. 1–2.
11. Song, J. Research on Leakage Current Sensor of Transformer Substation Capacitive Equipment Based on TMR. Master's Thesis, Harbin Industrial University, Harbin, China, 2021.
12. Hang, W.; Bing, H.; Yanqun, L.; Baofeng, N.; Bangdou, H. Phase current measurement method of three-core cable based on Surface Magnetic Field inversion. *Proc. CSEE* **2023**, 1–13. [CrossRef]

13. Wenkai, T.; Xin, T.; Haojie, Y. Non-contact current measurement device and Method based on TMR array. *Electr. Meas. Instrum.* 1–8. Available online: https://kns.cnki.net/kcms2/article/abstract?v=4wkQyjAcIEeMMersJfpwvo-iaKxbQ377-srDQJAoT5 rh7ByyqdJR_SmgsApVdXgy4V2XNMUyPWIJx6iIm7UJI-hpGFNHN85AA4OqGsfwRUZ0pBbFX63vV1WMkwliFQel1FX2Y9 bWaxqM36setN3_TZLDjnHFRTjBxXcyNU33HtpAEJ-CDxr3qf8hikxyVR6F&uniplatform=NZKPT&language=CHS (accessed on 20 June 2024).
14. Zhang, S. Effect of Phase Distance on Electromagnetic Environment of Overhead Transmission Lines. *Autom. Appl.* **2023**, *64*, 171–174.